Coriolis acceleration and critical slowing-down: A quantitative laboratory experiment

R. Mathevet[a)]
Laboratoire National des Champs Magnétiques Intenses, UPR 3228 CNRS/EMFL/INSA/UGA/UPS, Toulouse F-31400, France and IRES, Université Toulouse III, Toulouse F-31062, France

P. Marchou,[b)] C. M. Fabre,[c)] and N. Lamrani[d)]
IRES, Université Toulouse III, Toulouse F-31062, France

N. Combe[e)]
Centre d'Elaboration de Matériaux et d'Etudes Structurales, CNRS UPR 8011, 29 rue J. Marvig, BP 94347, 31055 Toulouse cedex 4, France and Université de Toulouse, UPS, F-31055 Toulouse, France

(Received 21 July 2022; accepted 26 September 2023)

We experimentally investigate the motion of a pendulum on a turntable. The dynamics of this conical pendulum experiment are very rich and can be studied both at the undergraduate and graduate levels. At low rotational frequency of the turntable, we measure the Coriolis acceleration. Increasing the rotational frequency, we experimentally demonstrate a supercritical pitchfork bifurcation: above a critical rotational frequency, the pendulum arm spontaneously rises up. Beyond the characterization of the equilibrium pendulum angle, we evidence the so-called critical slowing down corresponding to the increase in the pendulum period when approaching the critical rotational frequency. Bifurcation and critical slowing down are key concepts in the study of critical phenomena that are seldom illustrated experimentally. All our experimental measurements are in excellent quantitative agreement with the theory we provide.
https://doi.org/10.1119/5.0112643

I. INTRODUCTION

The conical pendulum[1–4] is a classic experiment used to illustrate Newton's laws to undergraduate students. A weight attached to the end of a string or rod is suspended from a fixed point and rotates around the vertical axis at rotational frequency Ω. In the simplest case, the pendulum makes a constant angle θ with the vertical axis so that the weight has a uniform circular path. The equations of motion can be derived either in the laboratory reference frame, assumed to be inertial, or in the non-inertial rotating reference frame, which then necessitates introducing inertial forces. For more advanced students, the same problem can be used to illustrate a pitchfork bifurcation in nonlinear physics: the stable equilibrium value of θ goes from zero to non-zero when the rotational frequency Ω exceeds a critical value Ω_c.[5] These two analyses of the conical pendulum focus on its equilibrium positions. In this manuscript, we propose to go further and investigate both theoretically and experimentally the dynamics of the pendulum, i.e., oscillations around its equilibrium position.

There are two types of conical pendulums with very different dynamics, depending on how they are linked to the suspension point. The first type employs a ball joint as for the Foucault pendulum.[6] We instead use the pendulums commonly found in undergraduate physics laboratories with a coupling that constrains the pendulum to swing in one plane. Our goal is to investigate the motion of such a pendulum set on a turntable. We report in this article two possible experiments that can be performed with this setup.

- *Measurement of the Coriolis acceleration for undergraduate students*
  Using Newton's laws in non-inertial frames of reference is usually difficult for undergraduate students. While they usually have a good intuition of centrifugal forces and sometimes of the Euler force, their understanding of the Coriolis force is most of the time limited to a mathematical formula. Its experimental illustration is usually limited to physical phenomena that can hardly be perceived and far away from everyday life: the eastward deflection of a projectile in the northern hemisphere,[7] the direction of rotation of cyclones,[8] or the Foucault's pendulum.[6] Indeed, tabletop experiments demonstrating the Coriolis force involve specific techniques that are usually difficult to implement in undergraduate physics laboratories.[9–11]
- *Pitchfork bifurcation and critical slowing down for graduate students*
  At a pitchfork bifurcation, by varying a control parameter (the rotational frequency Ω of the turntable in the present experiment), the system evolves from having one single stable state to exhibiting three equilibrium states, among which two are stable and one is unstable.[12] Pitchfork bifurcations are highly relevant, for instance to understand second order phase transitions using Landau's theory,[13] or, more generally, critical phenomena.[14] Before the system reaches the bifurcation point, its oscillation period increases as the system is drawn closer to the bifurcation threshold: this phenomenon is called the critical slowing down and is usually taught in courses on critical phenomena for graduate students.[15,16] While several experiments designed for undergraduate studies are available to illustrate pitchfork bifurcations,[5,17,18] critical slowing down is scarcely illustrated in graduate physics courses.[19]

An essential ingredient that makes our experiment relatively easy to implement is the use of on-board sensors.[20] They allow for easy and precise measurements of the 3D acceleration and of the 3D rotational frequency of the pendulum. We can use sensors associated with micro-controllers

such as Arduino for example. However, for ease of use, pedagogical attractiveness, and because mobile devices and sensors have recently shown their relevance for physics teaching,[21] we use a smartphone remotely controlled by the Phyphox app.[22] The smartphone serves as the pendulum's bob.[23] The measurements, transmitted by WiFi, are displayed in real time on a computer screen and are then processed by a data analysis software after the experiment.

This paper is organized as follows: After describing the experiment in Sec. II, we model it and derive the equations of motion in Sec. III. In Sec. IV, we give some details on the operating principle and measurements of the smartphone sensors. Then we report two of our experiments: the accurate measure of the Coriolis acceleration in Sec. V and the experimental study of a pitchfork bifurcation and of critical slowing down in Sec. VI.

II. EXPERIMENTAL SETUP

A pendulum is placed on a turntable, a freely rotating plate (Fig. 1(a)). Any freely rotating plate can be employed, but, in our setup, we used a spinning chair from which the seat has been removed. The legs of the chair (base of the turntable) are attached to the ground and assumed to be part of the ground in the following. The turntable can freely rotate around the vertical axis (Oz). The pendulum support is rigidly attached to the turntable so that at rest, the pendulum rod coincides with (Oz). The pendulum itself is composed of a rod, a smartphone and an extra weight used to adjust the oscillation period. Both the extra weight and the smartphone are rigidly attached to the end of the rod. In our case, the smartphone is inserted in an envelope that was taped to the rod.[23] The pendulum is constrained to rotate in an oscillation plane perpendicular to the horizontal axis (Ox') (Fig. 1(b)) which direction is determined by the rotation of the turntable. This latter constrain is a key feature of our setup as it will be shown in Sec. IV.

A typical experiment consists of first swinging the pendulum (around (Ox')) and then manually starting the rotation of the turntable (around (Oz)). The experimental setup is then left to evolve by itself: during that time, the smartphone sensors measure the acceleration and the angular velocity vectors. Since the turntable slows down relatively slowly compared to the pendulum, a single run allows exploration of a large range of angular velocities of the turntable, down to zero.

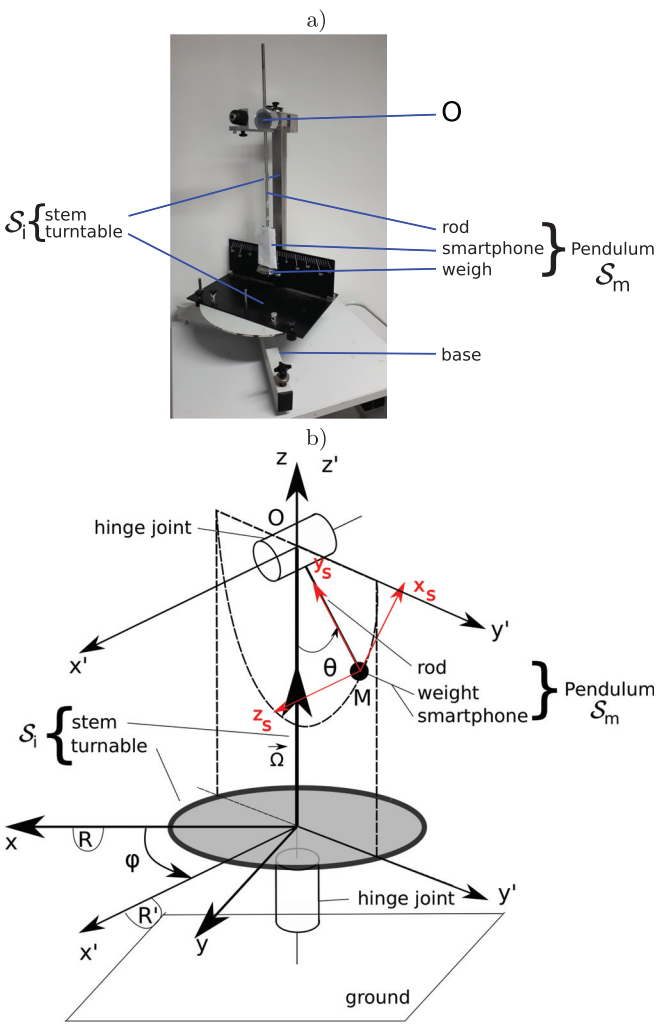

Fig. 1. (Color online) (a) Picture of the experiment. (b) Sketch of the experiment. The frame of reference (R) and (R') are, respectively, rigidly fixed to the ground and to the turntable.

III. MODEL AND EQUATIONS OF MOTION

A. Model

The Earth frame of reference (R) is considered as inertial since experiments last a few tens of seconds. $(Oxyz)$ defines the Cartesian coordinate system in (R), and $(\vec{e}_x, \vec{e}_y, \vec{e}_z)$ is its associated orthonormal basis. The frame of reference (R') is attached to the turntable with $(Ox'y'z')$ and $(\vec{e}_{x'}, \vec{e}_{y'}, \vec{e}_{z'})$ its associated Cartesian coordinate system and vector basis. (Ox') is parallel to the rotation axis of the pendulum arm oscillating in the $(Oy'z')$ plane. Axes (Oz) and (Oz') coincide. $\vec{\Omega}$ stands for the rotation vector of (R') (or of the turntable) with respect to (R) (the ground). In (R'), we distinguish (Fig. 1(b)):

- the immobile part $\mathcal{S}_i$ of the setup composed of the turntable and the stem: we model $\mathcal{S}_i$ by a solid body of moment of inertia I_s about the vertical axis (Oz).
- the mobile part $\mathcal{S}_m$ of the setup, namely, the pendulum composed by the rod, the smartphone, and the weight: $\mathcal{S}_m$ is modeled by a point mass m at point M at a distance l_0 from the hanging point O of the pendulum. Modeling $\mathcal{S}_m$ as a solid body and taking into account its principal moments of inertia is possible but leads to tedious calculations and unnecessarily complex expressions that complicate the interpretation.

The mechanical system studied in this manuscript, referred to as system below is composed of the two solid bodies $\mathcal{S}_i$ and $\mathcal{S}_m$. The joints between the two bodies $\mathcal{S}_i$ and $\mathcal{S}_m$ and the one between the body $\mathcal{S}_i$ and the ground, respectively, constrain their motions to a pure rotation along the axis $\vec{e}_{x'}$ and $\vec{e}_z$. In the modeling below, we neglect the fluid friction with air and solid friction at the pendulum mount and that of the spinning chair so that both joints correspond to perfect hinge (or revolute) joints.

The motion of the system which is deformable is described using the two independent degrees of freedom θ, the angle of the pendulum arm with respect to (Oz), and the angle of rotation of the turntable φ of the axis $\vec{e}_{x'}$ with

respect to the axis $\vec{e}_x$. We have, therefore, $\vec{\Omega} = \dot{\varphi}\vec{e}_z$, where the dot denotes the time derivative.

B. Equations of motion

The z-component L_z of the angular momentum of the system about (Oz) is a constant of the motion since the coupling connecting the turntable to the ground is assumed to be frictionless. The moment of inertia of the body $\mathcal{S}_m$ about (Oz) depends on θ: $I_p(\theta) = ml_0^2 \sin^2\theta$ so that, defining $I_{\text{tot}}(\theta) = I_s + I_p(\theta)$ the total moment of inertia of the system, the conservation of $L_z = I_{\text{tot}}(\theta)\Omega$ reads

$$\frac{dL_z}{dt} = \frac{d}{dt}\left[(I_s + ml_0^2 \sin^2\theta)\Omega\right] = 0, \tag{1}$$

from which we deduce a first equation of motion

$$(I_s + ml_0^2 \sin^2\theta)\dot{\Omega} + 2ml_0^2\Omega\dot{\theta}\sin\theta\cos\theta = 0. \tag{2}$$

The oscillation of the pendulum arm characterized by θ is, thus, coupled to the turntable's angular frequency Ω.

The time derivative of the work-energy theorem applied to the system reads

$$\frac{d}{dt}\left[\frac{1}{2}ml_0^2(\dot{\theta}^2 + \Omega^2\sin^2\theta) + \frac{1}{2}I_s\Omega^2\right] = P_{\text{int}} + P_{\text{ext}}. \tag{3}$$

The power P_{int} of internal forces cancels out due to the fact that the coupling between the pendulum arm and the stem is assumed to be frictionless. The power P_{ext} of external forces involves gravity, which is conservative, and the power dissipated at the coupling between the turntable and the ground, which is also assumed to be frictionless. Hence, P_{ext} reduces to the gravity contribution

$$\frac{d}{dt}\left[\frac{1}{2}ml_0^2(\dot{\theta}^2 + \Omega^2\sin^2\theta) + \frac{1}{2}I_s\Omega^2\right] = -mgl_0\dot{\theta}\sin\theta. \tag{4}$$

Combining Eqs. (2) and (4), we finally get

$$\ddot{\theta} + \omega_0^2\left[1 - \frac{\Omega^2}{\omega_0^2}\cos\theta\right]\sin\theta = 0, \tag{5}$$

where $\omega_0 = \sqrt{g/l_0}$ is the natural angular frequency of the pendulum. $\Omega_c = \omega_0$ is a critical angular frequency, and we will show in Subsection III C that it corresponds to the bifurcation angular frequency of the system. Equation (5) is similar to the equation of motion of a conical pendulum. However, as stated before, Ω is coupled to θ and, thus, evolves with time. Equations (2) and (5) are the equations we use in the following to understand the motion of the system.

C. The pitchfork bifurcation theory in a nutshell

The pitchfork bifurcation and the critical slowing down can be understood by introducing an effective potential.[24] As shown in the experimental sections below, the characteristic time of variation of Ω is about one order of magnitude larger than the period of the pendulum. As a consequence, we can assume Ω to be constant during an oscillation period. Equation (5) is then equivalent to the motion equation of a particle of mass m and position θ in an effective potential E_{eff},

$$E_{\text{eff}} = m\omega_0^2\left((1 - \cos\theta) - \frac{\Omega^2}{2\Omega_c^2}\sin^2\theta\right). \tag{6}$$

Incidentally for the system under consideration, the critical angular frequency Ω_c governing the pitchfork bifurcation is equal to ω_0 characteristic of the pendulum angular frequency, which is not necessarily the case in general. We, therefore, use both symbols in Eq. (6) to underline the qualitative difference between these two physical quantities. Approximating E_{eff} in Eq. (6) by its fifth-order Taylor expansion around 0, we get

$$E_{\text{eff}} \simeq \frac{1}{2}m\omega_0^2\left(\left((1 - \frac{\Omega^2}{\Omega_c^2}\right)\theta^2 - \frac{1}{12}\left((1 - 4\frac{\Omega^2}{\Omega_c^2}\right)\theta^4\right).$$

Figure 2(a) shows E_{eff} as a function of θ.

For $\Omega \leq \Omega_c$, E_{eff} only displays one minimum $\theta = 0$. From the curvature of E_{eff} in $\theta = 0$, we deduce the angular frequency ω of the pendulum swinging with a small amplitude around this minimum

$$\omega^2 = \omega_0^2\left(1 - \frac{\Omega^2}{\Omega_c^2}\right) \quad \text{for } \Omega \leq \Omega_c. \tag{7}$$

Hence, ω decreases as Ω increases and becomes zero at $\Omega = \Omega_c$, the critical rotational frequency. Conversely, the pendulum oscillation period increases when approaching Ω_c.

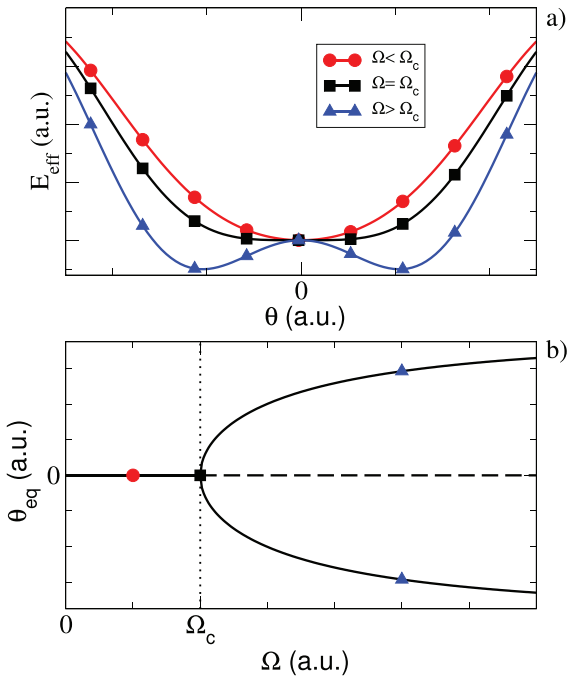

Fig. 2. (Color online) (a) Effective potential E_{eff} as a function of the pendulum angle θ for $\Omega < \Omega_c$ (solid red line with circle symbols), $\Omega = \Omega_c$ (solid black line with square symbols) and $\Omega > \Omega_c$ (solid blue line with triangle symbols). (b) Bifurcation diagram representing the equilibrium angles θ_{eq} as a function of the rotational frequency Ω. Solid and dashed lines, respectively, denote stable and unstable equilibrium angles.

This effect is called *critical slowing down*.[14,25] Note, however, that, while the oscillation period should diverge at $\Omega = \Omega_c$ according to Eq. (7), the fourth order term in Eq. (6) is then no longer negligible and the pendulum oscillations become anharmonic in the vicinity of Ω_c.

For $\Omega \geq \Omega_c$, the effective potential energy E_{eff} has two minima (Fig. 2(a)). The equilibrium angle $\theta = 0$ is unstable, and the pendulum arm spontaneously rises to a non-zero equilibrium angle θ_{eq} given by[4]

$$\cos\theta_{eq} = \frac{\Omega_c^2}{\Omega^2} \quad \text{for } \Omega \geq \Omega_c. \tag{8}$$

The evolution of the equilibrium angle θ_{eq} as a function of the rotational frequency Ω is represented in a bifurcation diagram (Fig. 2(b)) revealing the shape of a pitchfork.

IV. SMARTPHONE ACCELERATION AND ANGULAR VELOCITY

Mechanical sensors in smartphones are based on micro electromechanical systems (MEMS) attached to the smartphone body whose edges define the cartesian coordinate system (x_s, y_s, z_s). By construction, the axis z_s is perpendicular to the smartphone screen. In our experiments, we simultaneously use the three components of the acceleration $(a_{x_s}, a_{y_s}, a_{z_s})$ and of the angular velocity $(\omega_{x_s}, \omega_{y_s}, \omega_{z_s})$, which are measured with respect to the inertial frame of reference (R).[20,26,27]

The smartphone must be carefully positioned on the pendulum rod and oriented to facilitate further data analysis. We taped to the rod the envelope in which the smartphone is tightly inserted so that when the total system is at rest, the y_s-axis of the smartphone is vertical and coincides with the turntable rotation axis Oz, the x_s-axis lies in the oscillation plane $(Oy'z')$ and the z_s axis is parallel to the pendulum rotation axis Ox' (see Fig. 1).The accuracy of this setting can be controlled by measuring the acceleration vector from the MEMs in the smartphone (including gravity) when the total system is at rest. With this choice of orientations, the pendulum angular velocity $\dot{\theta}$ and the turntable rotational frequency Ω deduce from the measurements of the gyrometer following:

$$\dot{\theta} = \omega_{z_s} \quad \text{and} \quad \Omega = \sqrt{\omega_{x_s}^2 + \omega_{y_s}^2}. \tag{9}$$

The accelerations of the sensor positioned at point M[28] in both frames of reference (R) and (R') are related by

$$\vec{a}(M)|_{(R)} = \vec{a}(M)|_{(R')} + \vec{a_{ie}} + \vec{a_{ic}} \tag{10}$$

with the co-moving acceleration[29]

$$\begin{aligned}\vec{a_{ie}} &= \frac{d\vec{\Omega}}{dt} \times \vec{OM} + \vec{\Omega} \times (\vec{\Omega} \times \vec{OM}) \\ &= -l_0 \sin\theta \dot{\Omega} \vec{e_{x'}} - l_0 \Omega^2 \sin\theta \vec{e_{y'}}\end{aligned} \tag{11}$$

and the Coriolis acceleration

$$\begin{aligned}\vec{a_{ic}} &= 2\vec{\Omega} \times \vec{v}(M)|_{(R')} \\ &= -2l_0 \Omega \dot{\theta} \cos\theta \vec{e_{x'}}.\end{aligned} \tag{12}$$

The projection of Eq. (10) along (Ox') (equivalent to the z_s axis) is

$$\vec{a}(M)|_{(R)}.\vec{e_{x'}} = a_{z_s} = -l_0 \sin\theta \dot{\Omega} - 2l_0 \Omega \dot{\theta} \cos\theta \tag{13}$$

since $\vec{a}(M)|_{(R')}$ has no component along that axis.

As stated before and shown in Sec. V, the characteristic time of variation of Ω is about one order of magnitude larger than the period of the pendulum. We, therefore, neglect the first term in Eq. (13) (Euler acceleration) and keep only the second one (Coriolis acceleration).[30] To this approximation, a_{z_s} (Eq. (13)) measures the Coriolis acceleration.

In Sec. VI A, we will study the bifurcation of the system near the critical point. We, thus, need to obtain the equilibrium angle θ_{eq} from sensors measurements. In our experiment, Phyphox cannot directly provide an inclination measurement while recording the acceleration and angular velocity. To overcome this difficulty, we found the following solution to extract θ_{eq}. The gravity field, actually measured by the accelerometers, sets the vertical direction with respect to which θ is defined and may be retrieved from a_{x_s} and a_{y_s}. Indeed, on the one hand, we have

$$a_{x_s} = \vec{a}(M)|_{(R)}.\vec{e_{x_s}} - \vec{g}.\vec{e_{x_s}}, \tag{14}$$

$$a_{y_s} = \vec{a}(M)|_{(R)}.\vec{e_{y_s}} - \vec{g}.\vec{e_{y_s}}, \tag{15}$$

and on the other hand,

$$\vec{a}(M)|_{(R)}.\vec{e_{x_s}} = l_0\ddot{\theta} - l_0\Omega^2 \sin\theta\cos\theta, \tag{16}$$

$$\vec{a}(M)|_{(R)}.\vec{e_{y_s}} = l_0\dot{\theta}^2 + l_0\Omega^2 \sin^2\theta. \tag{17}$$

Projecting on the vertical axis (Oz) and combining these equations, we get

$$\sin\theta a_{x_s} + \cos\theta a_{y_s} = g + l_0\ddot{\theta}\cos\theta + l_0\dot{\theta}^2 \sin\theta. \tag{18}$$

When the equilibrium is reached, both $\dot{\theta}$ and $\ddot{\theta}$ are zero such that

$$\theta_{eq} = \arccos\left(\frac{g}{\sqrt{a_{x_s}^2 + a_{y_s}^2}}\right) + \arctan\left(\frac{a_{x_s}}{a_{y_s}}\right). \tag{19}$$

V. QUANTITATIVE ANALYSIS OF THE CORIOLIS ACCELERATION

A. Angular velocity variations

Let θ_0 denote the initial pendulum oscillation amplitude. The measurement of the Coriolis acceleration is done with small oscillation amplitudes $\theta_0 \ll 1$ and in the sub-critical regime $\Omega < \Omega_c$. Typically, for our pendulum $\omega_0 = \Omega_c \approx 5$ rad s^{-1}. We choose the initial conditions such that $\theta_0 \approx 0.25$ rad and $\Omega \approx 1.5$ rad s^{-1}.

Figures 3(a)–3(c) show the pendulum angular velocity $\dot{\theta}$, the turntable rotational frequency Ω, and the z-component of the acceleration a_{z_s} as a function of time, respectively. The two first quantities are deduced from the smartphone gyrometer measurements using Eq. (9). The amplitudes of $\dot{\theta}$ and Ω decrease with time due to the frictions at the hinge joints that have not been taken into account in the theoretical analysis of Sec. III. Friction at the joint between the stem and the rod of the pendulum is responsible for the decrease in the

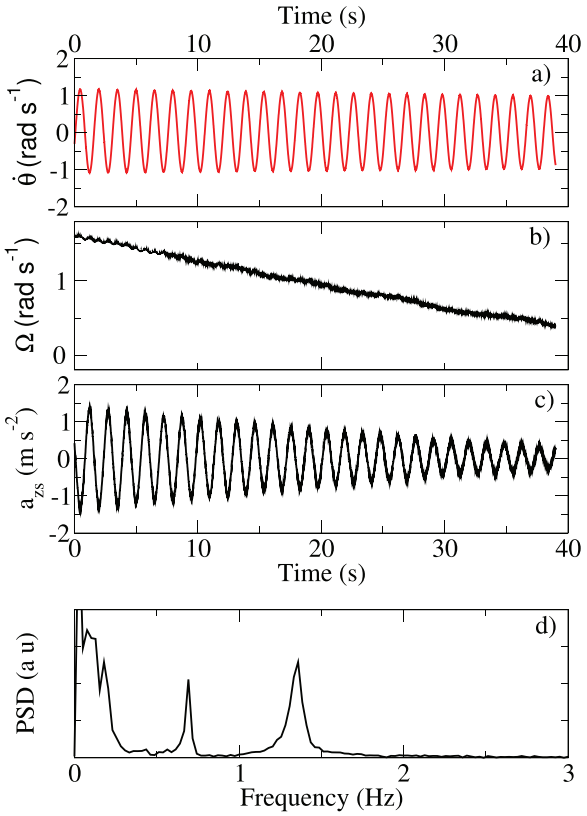

Fig. 3. (Color online) (a) and (b) Pendulum angular velocity $\dot{\theta}$ and turntable rotational frequency Ω as a function of time. (c) Acceleration a_{z_s} measured by the smartphone as a function of time. (d) Power spectral density of the subtraction of Ω from its linear regression.

amplitude of the pendulum angular velocity $\dot{\theta}$ while friction at the joint between the turntable and the ground is responsible for the decrease in turntable rotational frequency Ω. On the acquisition timescale, the dissipation effects are weaker on the pendulum angular velocity amplitude than on the turntable rotational frequency. In 15 oscillation periods of the pendulum ($\simeq 25$ s), the rotation frequency Ω decreases by a factor of 2: these different timescales justify that the co-moving acceleration can be neglected in Eq. (13) and that a_{z_s} can be identified with the Coriolis acceleration $-2l_0\Omega\dot{\theta}\cos\theta$.

In the small amplitude regime $\theta_0 \ll 1$, $\cos\theta \approx 1$ in Eq. (12) so that we plot in Fig. 4 a_{z_s} as a function of $\Omega\dot{\theta}$. From a linear regression, we get an estimate of the distance between the acceleration sensor and the pendulum axis $l_0^{\text{fit}} = 37.24 \pm 0.03$ cm. A direct measurement, with a ruler gives $l_0^{\text{ruler}} = 38.0 \pm 0.4$ cm. The relative difference between l_0^{fit} and l_0^{ruler} is about 2% and can be explained by the different approximations introduced in the model. To further verify the excellent agreement of the measurements with the model, it is also possible to compare the temporal evolutions of a_{z_s} and $-2l_0^{\text{fit}}\Omega\dot{\theta}$: the difference is hardly visible to the naked eye and is therefore not shown in Fig. 3(c).

A quantitative discussion of uncertainties is difficult: smartphone sensor specifications are available, but they are not useful because the detailed description of the software treatment of the raw data is usually not known.[31] The use of sensors dedicated to experimental physics driven by a microcontroller could, in principle, allow to circumvent this problem and to better control the measurement chain: the experimental setup and the data collection would, however, be more complex and presumably inappropriate for a teaching course.

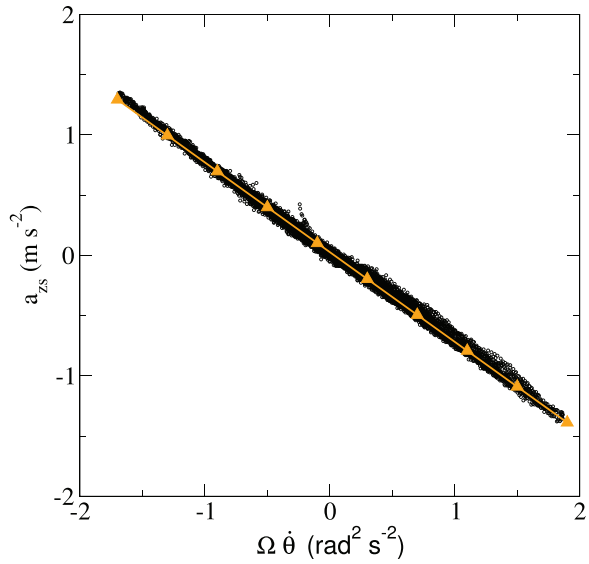

Fig. 4. (Color online) Acceleration a_{z_s} (black circle) as a function of $\Omega\dot{\theta}$ and its linear regression (orange line with triangle symbols).

Despite the absence of uncertainties estimations, our experimental setup yields an excellent agreement between model and measurements, allowing students to measure the Coriolis acceleration and to show its dependence on both on Ω and $\dot{\theta}$.

B. Back action on the turntable

A close inspection of Fig. 3(b) reveals small oscillations of the angular frequency Ω in addition to its quasi-linear decrease in time. These oscillations come from the variation of the total moment of inertia of the system $I_{\text{tot}} = I_s + ml_0^2\sin^2\theta$ as the pendulum swings. These oscillations occur at a frequency 2ω, as can be demonstrated using perturbation theory. At first order, the pendulum motion is harmonic: $\theta(t) = \theta_0\cos(\omega t)$. Using the conservation of the angular momentum component of the system $L_z = I_{\text{tot}}(\theta)\Omega$, we get in the small angle approximation

$$\Omega(t) = \frac{L_z}{I_s + ml_0^2\theta_0^2\cos^2(\omega t)} = \frac{L_z}{I_s + \frac{1}{2}ml_0^2\theta_0^2(1+\cos(2\omega t))}. \tag{20}$$

The pendulum oscillation frequency measured in Fig. 3(a) is 0.7 Hz and in agreement with Eq. (20), the spectrum of $\Omega(t)$ indeed exhibits a peak at 1.4 Hz as confirmed in Fig. 3(d) where, for sake of clarity, we have subtracted the linear trend of $\Omega(t)$ in order to compute the power spectral density. However, there is an almost equally intense peak at 0.7 Hz that is not predicted by our model. We believe that this is due to a slight misorientation of the smartphone. Indeed, if the z_s axis does not perfectly coincide with (Ox'), a small component of $\dot{\theta}\vec{e_{x'}}$ projects on the x_s and y_s axes giving rise to a 0.7 Hz term in the time evolution of $\Omega = \sqrt{\omega_{x_s}^2 + \omega_{y_s}^2}$. Hence, the pendulum swings affect the rotation of the turntable.

VI. PITCHFORK BIFURCATION AND CRITICAL SLOWING DOWN

A. Pitchfork bifurcation diagram

In this section, we experimentally measure the bifurcation diagram, i.e., the equilibrium angle θ_{eq} of the pendulum as a function of the rotational frequency Ω of the turntable.[4] Since it is very difficult to impose rotational frequency Ω without any pendulum swing, we add a solid friction in order to damp the pendulum oscillations in typically 10 s.[32] With the pendulum at rest, we gradually increase Ω by pulling on a string wound around the turntable. When we cross the critical point Ω_c, the pendulum moves suddenly away from $\theta_{eq} = 0$ and settles after a few oscillations to a non-zero angle. We then start the data acquisition. Since Ω is slowly decreasing due to friction between the turntable and the ground, the system then successively investigates regimes above and below the bifurcation. We then use Eq. (19) to compute θ_{eq} and then plot it as a function of Ω (Fig. 5(a)).

For this experiment, we have used a slightly different pendulum with $\omega_0 \approx 3.55\,\text{rad.s}^{-1}$. Using Eq. (8), a nonlinear fit of θ_{eq} as a function of Ω above the bifurcation threshold provides a measurement of $\Omega_c \approx 3.5$ rad s^{-1} in agreement within a few percent with the natural angular frequency ω_0 of the pendulum. Moreover, above the threshold, Eq. (8) predicts a linear dependence of $\cos\theta_{eq}$ on $1/\Omega^2$ with slope Ω_c^2 Fig. 5(b). We get $\Omega_c^{\text{fit}} = 3.565$ rad s^{-1} using a linear regression (orange line). This value is consistent, again within a few percent, with the previous determination.

B. Critical slowing down

In this section, we study the critical slowing-down using a system with $\omega_0 = 4.92$ rad s^{-1} similar to the one used in Sec. V, i.e., released from the artificial friction used in Sec. VI A. We use the same launching procedure and measurements protocol as in Sec. VI A with initial conditions $\Omega \sim 7$ rad s^{-1}. Figures 6(a) and 6(b) show the pendulum angular velocity $\dot{\theta}$ and the turntable rotational frequency Ω as a function of time.

We analyze numerically $\dot{\theta}$ to detect its zero-crossing times from which we compute the instantaneous period T of the pendulum[23] (Fig. 6(c)). The period is clearly diverging at time $t_c = 19$ s, evidencing the presence of a bifurcation and of a critical slowing down. We measure in Fig. 6(b) $\Omega_c = \Omega(t_c) = 4.9$ rad s^{-1}, which agrees within less than a percent with the natural angular frequency $\omega_0 = 4.92$ rad s^{-1} of the pendulum that we used for this experiment.

To go beyond, we compute the oscillation instantaneous angular frequency $\omega = 2\pi/T$ and compare it to Eq. (7) that predicts an affine relationship between ω^2 and Ω^2 (Fig. 7) with slope –1 (dashed line) for $\Omega \leq \Omega_c$. The agreement at low rotational frequencies is good but degrades approaching the bifurcation threshold. There, the approximations we have made, noticeably the harmonic one, break down. Moreover, near the threshold, all experimental imperfections, such as the smartphone misorientation or the mispositionning of the pendulum, are magnified. Far enough from the bifurcation in the subcritical regime ($\Omega \lesssim 4$ rad s^{-1} in this case), we observe a quantitative agreement of the measurements with the model.

C. Rotational frequency variations

Similarly to Sec. V, we can analyze the back action of the pendulum oscillations on the rotational frequency of the

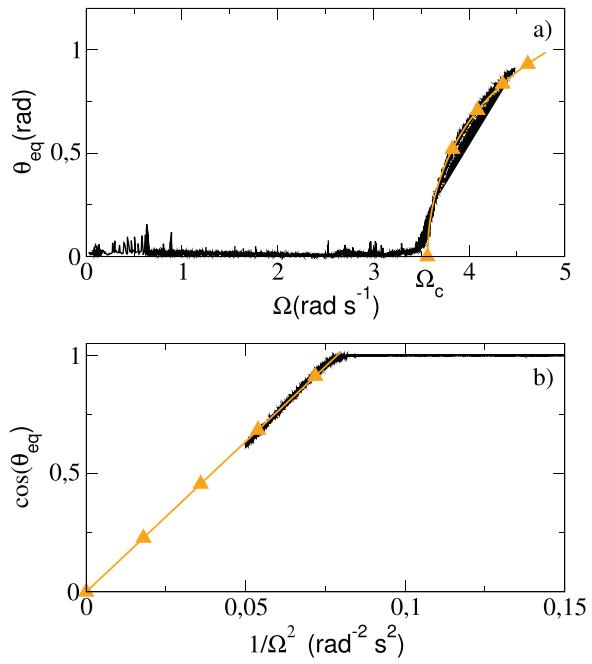

Fig. 5. (Color online) (a) Equilibrium angle of the pendulum as a function of Ω (black line) compared to the theoretical prediction (Eq. (8)) (orange line with triangle symbols). (b) Cosine of the equilibrium angle of the pendulum as a function of $1/\Omega^2$ (black line) and its linear regression (orange line with triangle symbols).

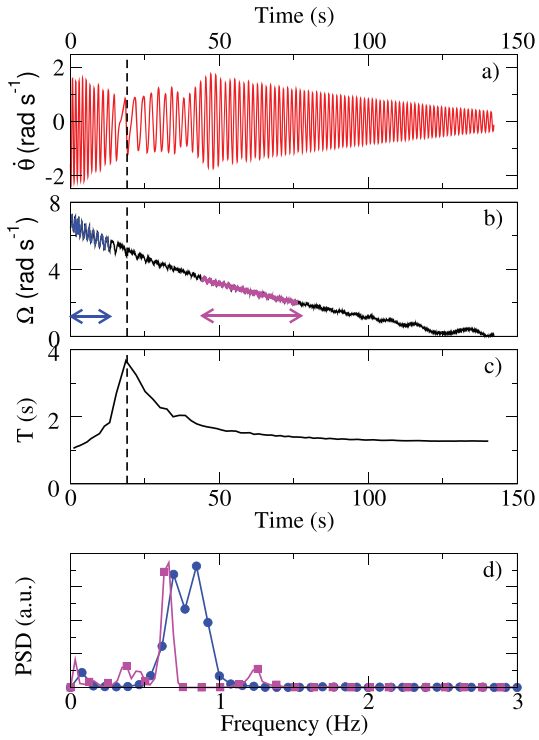

Fig. 6. (Color online) (a) and (b) Pendulum angular velocity $\dot{\theta}$ and turntable rotational frequency Ω as a function of time. The dashed line features the occurrence of the bifurcation. The spectral analysis in (d) is performed on the time ranges denoted by the double arrows. (c) Period T of the pendulum as a function of time. (d) Power spectral density of the subtraction of Ω from its linear regression for $0 < t < 13$ s (solid blue line with circle symbols) and for $44 < t < 76$ s (solid magenta line with square symbols).

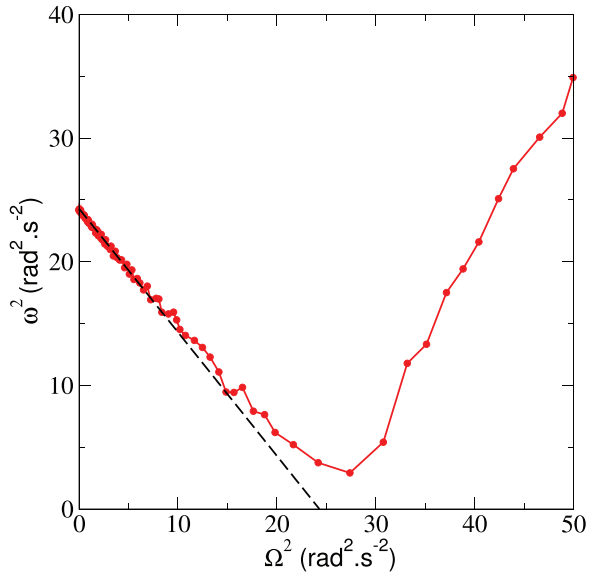

Fig. 7. (Color online) Square of the pendulum angular velocities ω^2 (red solid line) and sub-critical prediction (dashed solid line) Eq. (7) as a function of Ω^2.

turntable. We extract from the Ω time series two samples denoted on Fig. 6(b). They correspond to times $0 < t < 13$ s and $44 < t < 76$ s, respectively, below and above the threshold ($t_c = 19$ s). Figure 6(d) shows the Fourier transform of these two samples. Because the sample duration is reduced, the peaks are relatively broad and the result is less pronounced than that of Fig. 3(d). Below the bifurcation (magenta with square symbols), we observe two peaks at 0.64 and 1.24 Hz, while above the bifurcation (blue with circle symbols), we observe only a single broad peak at about 0.75 Hz. Using the same perturbative approach as in Sec. V, we have in the supercritical regime $\Omega > \Omega_c$, at first order, $\theta(t) = \theta_{eq} + \theta_0 \cos(\omega t)$ with $\theta_0 \ll \theta_{eq}$. A Taylor expansion of I_{tot} then yields

$$\begin{aligned} I_{\text{tot}} &= I_s + ml_0^2 \sin^2\theta(t) \\ &\simeq I_s + ml_0^2 \left[\sin^2\theta_{eq} + \theta_0 \cos(\omega t) \sin 2\theta_{eq} \right], \end{aligned}$$

which gives just one peak at angular frequency ω in agreement with the observation. The presence of two peaks at 0.64 and 1.24 Hz below the threshold is explained in the same way as in Sec. V B.

VII. CONCLUSION AND OUTLOOK

We have characterized the motion of a pendulum set on a turntable by recording the accelerations and angular velocities with a smartphone attached to the pendulum arm. This simple setup has turned out to be really valuable:

- It allows a quantitative experimental measurement of the Coriolis acceleration according to the model that we provide. Undergraduate students are thus able to better grasp the difficult concept of inertial force.
- At a more advanced level, the quantitative analysis of the critical slowing down below a pitchfork bifurcation experimentally illustrates the deep but often abstract concepts of courses on critical phenomena.

Contrary to previously reported systems evidencing the same physic phenomena, our setup is fairly easy to implement in any undergraduate physics lab, without even needing to purchase additional equipment in most cases. This experiment has been carried out by all of our students who plan a career in undergraduate physics teaching: their main difficulties were to assimilate the model and its resolution and to clearly understand what the smartphone sensors measured.

These experiments could be improved by using specific sensors dedicated to experimental physics in order to perform uncertainty analysis. To go beyond, an examination of the supercritical regime $\Omega > \Omega_c$ in Fig. 7 could be considered: experimental measurements could be compared to numerical simulations of Eqs. (2) and (5) to experimentally deduce the ratio ml_0^2/I_s. The comparison of this ratio with the experiment would however require to properly model the system using a solid-body pendulum.

AUTHOR DECLARATIONS

Conflict of Interest

The authors have no conflicts of interest to disclose.

APPENDIX: MATERIAL

The pendulum that has been used for these experiments is Nova-Physics ref. MOP050.[33] The smartphone is a Samsung Galaxy A5 with an accelerometer and gyrometer K6DS3TR provided by STM. Finally, the turntable is derived from a spinning chair formerly sold by Leybold.

[a]ORCID: 0000-0003-2272-5718.
[b]ORCID: 0000-0002-1998-7779.
[c]ORCID: 0000-0002-4957-0974.
[d]ORCID: 0000-0003-2044-8542.
[e]Electronic mail: nicolas.combe@cemes.fr, ORCID: 0000-0003-0582-2970.

[1]H. R. Bambill, M. R. Benito, and G. R. Garda, "Investigation of conservation laws using a conical pendulum," Eur. J. Phys. **25**(1), 31–35 (2004).
[2]S. S. Tongaonkar and V. R. Khadse, "Experiment with conical pendulum," Eur. J. Phys. Educ. v(1), 1–6 (2011); available at http://www.eu-journal.org/index.php/EJPE/article/view/129.
[3]J. A. Giacometti, "The motion of a conical pendulum in a rotating frame: The study of the paths, determination of oscillation periods, and the Bravais pendulum," Am. J. Phys. **88**(4), 292–297 (2020).
[4]L. Minkin and D. Sikes, "Demonstrating conical pendulum stable and unstable states," Phys. Teach. **59**(6), 474–476 (2021).
[5]N. Sungar, J. P. Sharpe, M. J. Moelter, N. Fleishon, K. Morrison, J. McDill, and R. Schoonover, "A laboratory-based nonlinear dynamics course for science and engineering students," Am. J. Phys. **69**(5), 591–597 (2001).
[6]L. Foucault, "Physical demonstration of the rotational motion of the Earth by means of the pendulum" C. R. Acad. Sci., **32**, 135–138 (1851) (in French).
[7]O. E. Thompson, "Coriolis deflection of a ballistic projectile," Am. J. Phys. **40**(10), 1477–1483 (1972).
[8]J. R. Holton, *An Introduction to Dynamic Meteorology* (Academic Press, Cambridge, MA, 1992), Chap. 1, 3rd ed.
[9]A. M. Martin and D. F. Mariani, "Coriolis acceleration: A laboratory experiment," Am. J. Phys. **52**(9), 814–817 (1984).
[10]T. Lewowski, L. Lewowska, and P. Mazur, "Measurement of the effect of Coriolis and centrifugal forces on the trajectory of a body in a rotating frame," Eur. J. Phys. **20**(2), 109–116 (1999).
[11]A. Shakur and J. Kraft, "Measurement of coriolis acceleration with a smartphone," Phys. Teach. **54**(5), 288–290 (2016).
[12]J. R. Tredicce, G. L. Lippi, P. Mandel, B. Charasse, A. Chevalier, and B. Picqué, "Critical slowing down at a bifurcation," Am. J. Phys. **72**(6), 799–809 (2004).

[13]L. Landau and E. Lifchitz, *Statistical Physics* (Mir, Moscou, 1980), Chap. 142, 2nd ed.
[14]P. M. Chaikin and T. C. Lubensky, *Principles of Condensed Matter Physics* (Cambridge U. P., Cambridge, 1995), Chap. 8.
[15]M. Scheffer, J. Bascompte, W. A. Brock, V. Brovkin, S. R. Carpenter, V. Dakos, H. Held, E. H. van Nes, M. Rietkerk, and G. Sugihara, "Early-warning signals for critical transitions," Nature **461**(7260), 53–59 (2009).
[16]M. Gomez, D. Moulton, and D. Vella, "Critical slowing down in purely elastic 'snap-through' instabilities," Nat. Phys. **13**(2), 142–145 (2017).
[17]J. P. Sharpe and N. Sungar, "Supercritical bifurcation in a simple mechanical system: An undergraduate experiment," Am. J. Phys. **78**(5), 520–523 (2010).
[18]F. Moisy, "Supercritical bifurcation of a spinning hoop," Am. J. Phys. **71**(10), 999–1004 (2003).
[19]J. Bobnar, K. Susman, V. A. Parsegian, P. R. Rand, M. Čepič, and R. Podgornik, "Euler strut: A mechanical analogy for dynamics in the vicinity of a critical point," Eur. J. Phys. **32**(4), 1007–1018 (2011).
[20]R. Bogue, "Recent developments in MEMS sensors: A review of applications, markets and technologies," Sens. Rev. **33**(4), 300–304 (2013).
[21]M. Monteiro and A. C. Mart, "Resource letter MDS-1: Mobile devices and sensors for physics teaching," Am. J. Phys. **90**(5), 328–343 (2022).
[22]"Phyphox," www.phyphox.org.
[23]R. Mathevet, N. Lamrani, L. Martin, P. Ferrand, J. P. Castro, P. Marchou, and C. M. Fabre, "Quantitative analysis of a smartphone pendulum beyond linear approximation: A lockdown practical homework," Am. J. Phys. **90**(5), 344–350 (2022).
[24]P. Manneville, *Instabilities, Chaos and Turbulence*, 2nd ed. (Imperial College Press, London, 2010), Chap. 2.
[25]D. Forster, *Hydrodynamic Fluctuations, Broken Symmetry, and Correlation Functions* (Perseus Books, New York, NY, 1990). Chap. 2.
[26]L. Roylance and J. Angell, "A batch-fabricated silicon accelerometer," IEEE Trans. Electron Devices **26**(12), 1911–1917 (1979).
[27]V. M. N. Passaro, A. Cuccovillo, L. Vaiani, M. De Carlo, and C. E. Campanella, "Gyroscope technology and applications: A review in the industrial perspective," Sensors **17**(10), 2284–2306 (2017).
[28]The position S of the acceleration sensors of a smartphone does generally not coincide with its center of mass. If S does not coincide with M, the coordinates of M (OM, θ, φ) should be replaced in the calculation by coordinates of S $(OS, \theta_s, \varphi_s)$.
[29]The co-moving acceleration is the acceleration that the point M would have relative to (R) if it was at rest in (R').
[30]Conversely, if $\vec{v}(M)|_{(R')} = \vec{0}$ the Coriolis acceleration is zero, one can measure along the x'-axis the Euler acceleration during the acceleration and deceleration phases of the turntable rotation.
[31]D. S. Odenwald, *A Guide to Smartphone Sensors*, edited by NASA (NASA Space Science Education Consortium, Houston, TX, 2019).
[32]The rod of the pendulum that we use is attached to a cylinder $\mathcal{C}_m$ that can rotate in a cylindrical part $\mathcal{C}_i$ of the stem through ball bearings. In order to add some friction on that coupling, a plastic lamella fixed on the cylindrical part $\mathcal{C}_i$ of the stem scrapes on the cylinder $\mathcal{C}_m$.
[33]"Nova physics," https://www.nova-physics.com.

Small Vacuum Pump

Most late nineteenth century vacuum pumps were large affairs, with one or two cylinders and an attachment for a manometer to measure the extent of the vacuum. This small syringe pump was photographed in 1999 at the Callan Museum at St. Patrick's College in Maynooth, Ireland. Mollan (Charles Mollan and John Upton, The Scientific Apparatus of Nicholas Callan and Other Historical Instruments (St. Patrick's College, 1994) pg 239) notes that the system resembles that of the ordinary bicycle pump, although running in reverse. (Picture and text by Thomas B. Greenslade, Jr., Kenyon College)